Journal of the Oceanographical Society of Japan
Vol. 27, No. 5, pp. 218 to 232, October 1971

# Wave Particle Velocities Measured with a Doppler Current Meter*

Keisuke TAIRA**

**Abstract:** A newly developed three-dimensional Doppler current meter is described and the results of preliminary field experiments are presented where simultaneous measurements of surface elevation and water velocity associated with wave orbital motion were made. The phase difference between the surface elevation and the vertical velocity measured at 1.0 and 0.45 meters below the mean water level is found to be approximately 90°, in accord with the theory for surface waves of infinitesimally small amplitudes. The spectral (frequency) density distribution for velocity is also found to agree with that we would expect from the linear theory for the observed frequency distribution of surface elevation. However, the amplitude of velocity is consistently smaller (about 10 %) than that we would expect. This reduction of amplitude is more pronounced in cases where waves are high and the water depth is shallow.

## 1. Introduction

It is well known that many characteristics of ocean waves are accounted for by the theory for surface waves of infinitesimally small amplitudes, but the orbital motion associated with these waves does not produce the Reynolds stress. In reality, however, the Reynolds stress is known to be acting in the appreciable magnitude in the upper portion of the ocean. The direct measurements of the vertical flux of horizontal momentum (Reynolds stress) have recently been made by SHONTING (1964, 1967, 1968, 1970) and YEFIMOV and KHRISTOFOROV (1969) with cylindrical impeller-driven ducted current meters. They found that the most part of the Reynolds stress was produced by orbital motions of waves over the frequency range near the spectral peak. More surprisingly, they found that the Reynolds stress in the upper ocean is about ten times in magnitude the Reynolds stress observed in the air close to the sea surface.

Also important to the air-sea interaction problem is the growth rate of oceanic waves. The motion in the ocean such as waves and currents is caused, at least partly, by the wind blowing over the sea surface which imparts its momentum to water. The theories have been advanced to predict the wave generation and development (PHILLIPS, 1966). The observational results by SNYDER and COX (1966), however, show that the actual growth rate of waves is about ten times larger than that predicted by Miles' model. Estimating the wave drag, *i.e.*, the momentum flux into the waves, from the observed growth rate, they found that the wave drag is about seven times larger than that in the air close to the sea surface. More recent observations of the growth rate of waves by BARNETT and WILKERSON (1967) and IWATA and TANAKA (1970) agree with Snyder and Cox's results.

The observational result described above indicates that much remains to be investigated to increase our understanding of the physical process associated with the momentum flux across the sea surface and to understand the momentum balance in the combined system of surface boundary layers in the atmosphere and ocean.

A research group at the Ocean Research Institute, the University of Tokyo, has initiated a field experiment program designed to measure simultaneously and directly momentum fluxes

* Received September 20, 1971
** Ocean Research Institute, University of Tokyo, Nakano, Tokyo, 164 Japan

in air and in water with sonic anemometers, capacitance wave gauges and a Doppler current meter, (TAIRA, 1971). The Doppler current meter is a fast-responding current meter which has been newly developed. The purpose of this paper is to describe the Doppler current meter and to present the preliminary result obtained with it. The discussion of the result will be confined to the comparison of the observed result with the theory of waves of infinitesimally small amplitudes.

## 2. A Doppler current meter

Velocity fluctuations of our interest are those associated with orbital motions of wind waves or swells, turbulence and wind currents. They cover a wide frequency band ranging from almost D.C. to very high frequency. We confine our interests mainly in the frequency band of wind waves and 10 Hz is selected as the highest frequency for a current meter. The full scale of the meter is chosen to be $\pm 200$ cm/sec so that orbital motions of fully-developed wind waves under the wind of about 15 m/sec speed can be measured. Moreover, the shape of the sensors is severely required not to disturb the velocity field to measure fluctuations of small scale with high accuracy.

After examining several kinds of current meter which have been developed previously by other authors, we have chosen a Doppler current meter as the one which would meet these requirements. One-dimensional Doppler current meter had already been developed by KOCZY, KRONENGOLD and LOEWENSTEIN (1962), KRONENGOLD and VLASAK (1965).

An operational principle of the current meter is based on the Doppler effect of sonic waves. A crystal-controlled oscillator drives a piezoelectric disc transmitter at a frequency of 10.65 MHz. The diameter of the disc is 1.0 cm and the beam is very sharp (1° at the half power point). Emitted sound waves are scattered by particulate matter which is assumed to be moving with the ambient fluid's velocity. Scattered sonic waves are received by a piezoelectric disc receiver whose beam is focused on the way of transmitter's beam (Figure 1). Focused sphere, approximately 8 mm cube

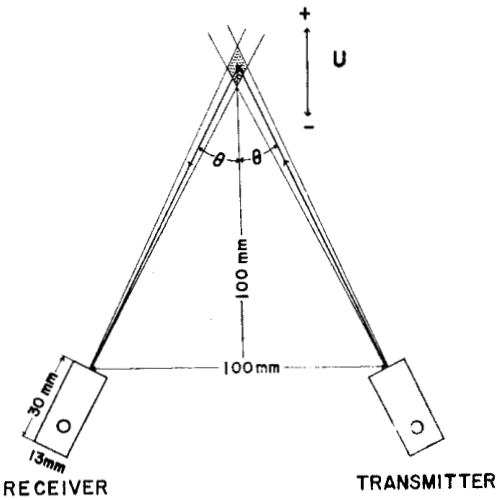


Fig. 1. A schematic of a pair of transducers for the Doppler current meter.

according to our examination in a test tank with a wire of 1 mm in diameter, is 11 cm apart from both the transmitter and the receiver.

Let $U$ be the fluid's velocity (Figure 1), then the frequency of received sound waves $f_R$ is of the form (KRONENGOLD and VLASAK 1965):

$$f_R=\frac{C-U\cos\theta}{C+U\cos\theta}f_T \qquad (1)$$

where $f_T$ is the frequency of emitted sound waves, $C$ is sound velocity in the water and $\theta$ ($=26°34'$) is the angle between fluid's velocity and the transmitter. The angle between the velocity and the receiver is also $\theta$. The frequency difference $\Delta F$ is readily found to be

$$\Delta F=f_T-f_R=\frac{2U\cos\theta}{C+U\cos\theta}f_T$$

Generally the sound velocity is much larger than the fluid's velocity, i.e., $C\gg|U\cos\theta|$ and the frequency difference can be rewritten as

$$\Delta F=\frac{2f_T}{C}U\cos\theta \qquad (2)$$

The sign of $\Delta F$ is in accordance with that of the fluid's velocity. Then by detecting the frequency difference, we can calculate the fluid's velocity by the equation.

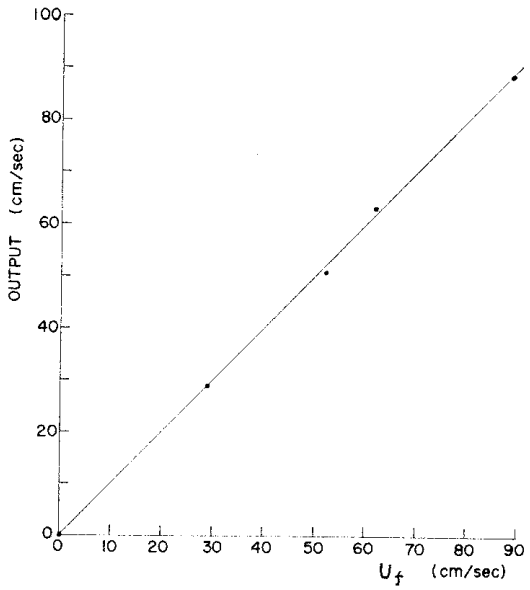


Fig. 2. Speed characteristics of the Doppler current meter where $U_f$ is the velocity of the frame.

Three pairs of the trasmitters and the receivers are used to measure three components of the fluid's velocity vector at a space point.* The components of velocity are measured by a time shearing method at a rate of 300 cycles per second. The method is advantageous because only one crystal-controlled oscillator is needed for transmitters of the three components, and transducers as well as some electric circuits can be consisted with parts of the same standard. Pulse number modulation is used to detect the frequency difference $\Delta F$. Firstly a frequency $\delta F$ is generated by adding 50.0 KHz to $\Delta F$ with some devices. Then $\delta F$ is always positive and proportional to the velocity $U\cos\theta$. By rectifying the signals, pulses are generated for 1.0 millisecond and the number of the pulses is proportional to the frequency $\delta F$. After demodulation, voltage signal is fed into a low pass filter and then to the meter read out, and also to the output for recording. Although quantizing error in the measurement of 1.0 millisecond is about 7 cm/sec, it is reduced to about 0.2 cm/sec after averaging for 100 milliseconds by the low pass filter. Electric calibration af the meter is made by using a frequency controlled by a crystal oscillator.

The Doppler current meter was calibrated in a wooden test tank of 80 cm long, 60 cm wide and 40 cm deep. The current meter was suspended from a moving frame and was reciprocated in the tank. The amplitude of the reciprocation was fixed at 15 cm and the period was changed. The speed characteristic curve of the meter is shown in Figure 2. The curve shows good linearity. Deviations of the measured values are less than 1 cm/sec and they are mainly caused by the erratic movement of the frame.

* Another method is available. WISEMAN (1969) developed a three-dimensional Doppler current meter with one transmitter and three receivers.

## 3. Wave particle velocities for infinitesimal-amplitude waves

Before describing the result of our observations, it is instructive to summarize some characteristics of surface waves of infinitesimally small amplitudes.

Let $\eta$ be the surface elevation expressed by

$$\eta = a\cos(\boldsymbol{k}\cdot\boldsymbol{x}-\sigma t) \qquad (3)$$

where $\boldsymbol{k}=k_x\boldsymbol{i}+k_y\boldsymbol{j}$ is wave number vector and $\sigma$ is angular frequency of the waves. The horizontal coordinates $\boldsymbol{x}=x\boldsymbol{i}+y\boldsymbol{j}$ ($\boldsymbol{i}$ and $\boldsymbol{j}$ are orthogonal unit vectors) are placed on the undisturbed free surface. The vertical $z$-axis is taken upward positive. For infinitesimal-amplitude waves whose wave amplitude $a$ is smaller than both the wavelength and the water depth, the wave particle velocities are of the forms (PHILLIPS, 1966):

$$\boldsymbol{u}=\frac{\boldsymbol{k}}{|\boldsymbol{k}|}\frac{\sigma a\cosh|\boldsymbol{k}|(z+d)}{\sinh|\boldsymbol{k}|d}\cos(\boldsymbol{k}\cdot\boldsymbol{x}-\sigma t) \qquad (4)$$

$$w=\frac{\sigma a\sinh|\boldsymbol{k}|(z+d)}{\sinh|\boldsymbol{k}|d}\sin(\boldsymbol{k}\cdot\boldsymbol{x}-\sigma t) \qquad (5)$$

and the dispersion relation is given by

$$\sigma^2=g|\boldsymbol{k}|\tanh|\boldsymbol{k}|d \qquad (6)$$

where $g$ is the gravitational acceleration and $d$ is the water depth. The amplitude ratio be-

tween the vertical velocity and the surface elevation reduces to:

$$\left|\frac{w}{\eta}\right| = H(|\boldsymbol{k}|, d, z)\cdot\sigma \qquad (7)$$

where $H(|\boldsymbol{k}|, d, z)$ is hydraulic filter of the form:

$$H = \frac{\sinh|\boldsymbol{k}|(z+d)}{\sinh|\boldsymbol{k}|d} \qquad (8)$$

For the values of parameters $d=20.0$ meters and $z=-1.0$ meter calculated from (6), (7) and (8), the values of $H$, $\sigma$ and $\left|\frac{w}{\eta}\right|$ are plotted against the frequency $f(=\sigma/2\pi)$ in Figure 3 on a log-log scale. The slope of the amplitude ratio $\left|\frac{w}{\eta}\right|$ decreases as wave frequency becomes higher. This ratio will be compared with the observational results in the following section.

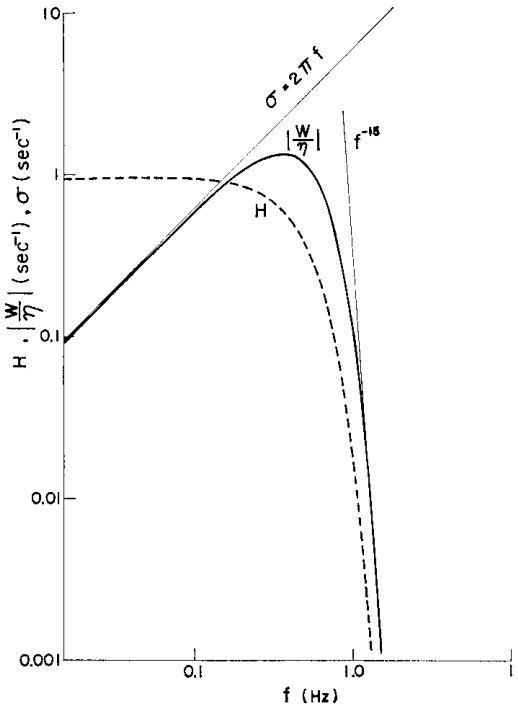


Fig. 3. The hydraulic filter H, and the amplitude ratio of the vertical velocities to that of the surface elevation against the wave frequency, evaluated at 1.0 meter beneath the water surface for infinitesimal-amplitude waves propagating in the 20.0 meters deep water.

## 4. Observational results

Several series of observations were carried out at a marine tower located to the south of the shore in the Bay of Sagami. The distance from the shore is about 1 km where the water depth is 20.0 meters. The shoreline is almost straight line about 50 km extending in the east-west direction. Figure 4 shows the eastward view of the marine tower, where observational arrangement was made on a frame swiveling to the south.

The observational arrangement is shown in Figure 5. Measurements were carried out at the frame end 4 meters apart from one basis of the tower. The Doppler current-meter (Figure 6) was attached to a pole and immersed 1.0 meter beneath the sea surface. On the top of the same pole, a sonic anemometer was set at 3.8 meters above the sea surface. A

Fig. 4. The eastside view of the Hiratsuka Marine Observation Tower (National Reseach Center for Disaster I revention) located in the Bay of Sagami.

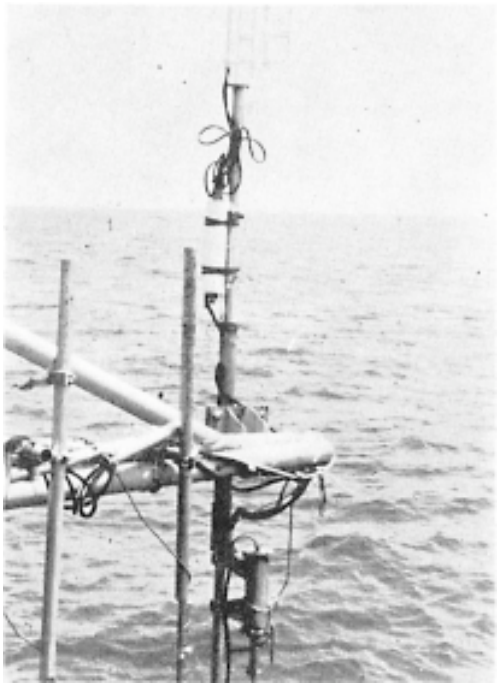

Fig. 5. Observational arrangement made on the swiveling frame of the tower.

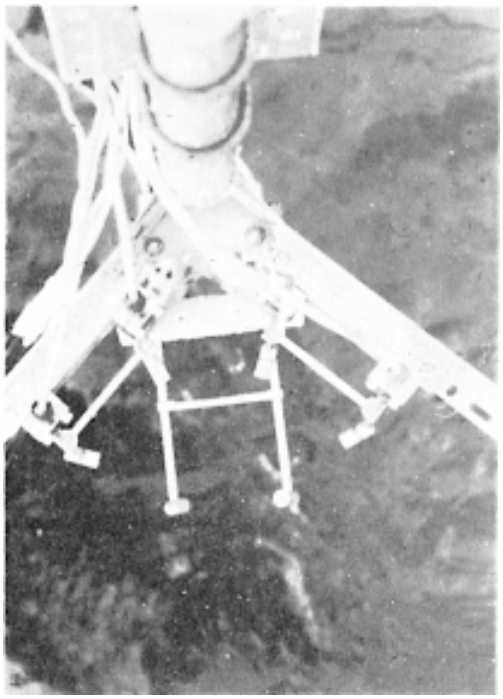

Fig. 6. Sensors of the three-dimensional Doppler current meter.

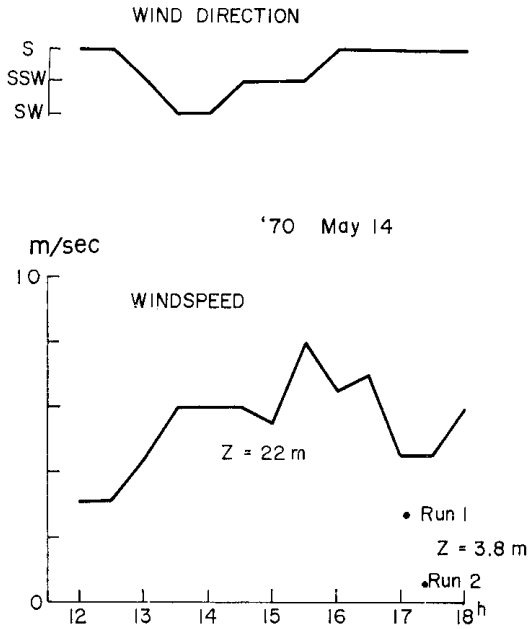


Fig. 7. Wind data during the observations.

wire-capacitance wave gauge was also attached to the pole.

Signals of the wave gauge, current-meter and sonic anemometer were recorded on magnetic tape. On playback, these analog signals were digitized and punched on paper tapes for a computer. Spectral analysis was made digitally, using an algorithm of Fast Fourier Transform and the method is described in Appendix.

The wind condition on May 14 in 1970 when the observation was carried out is shown in Figure 7. The wind was measured on the top of the tower 22 meters above the sea surface with an anemometer of vane type. The observed data were read out every half an hour. Wind was blowing from the south during the observation. Mean wind speed measured by the sonic anemometer is plotted in the same figure by a dot. The wind speeds at 3.8 meters height were converted into the speeds at 22 meters height assuming the "log-law" with the roughness length of 0.2 cm and found 3.1 m/s for the Run 1 (17:10–17:20) and 1.0 m/s for the Run 2 (17:20–17:30). The observation was made in a transient state.

The power spectra computed from the data on May 14 are shown in Figures 8 and 9. The

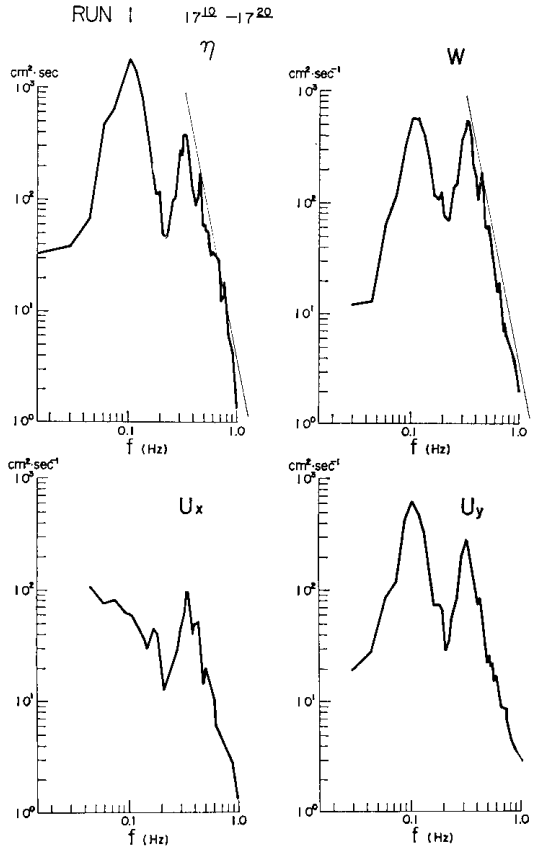


Fig. 8. Observed power spectra for the Run 1: $\eta$··· the surface elevation, $w$··· the vertical velocities, $U_x$··· the horizontal velocities of the $x$-component, $U_y$··· the horizontal velocities of the $y$-component.

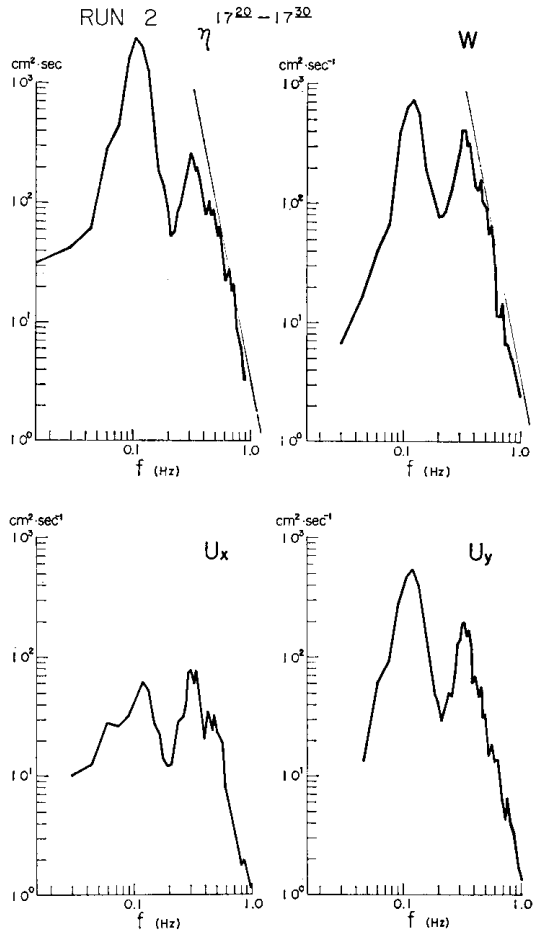


Fig. 9. Observed power spectra for the Run 2: see the caption to Figure 8.

sampling time interval was 0.32 seconds and the number of data in one series of record was 2048. In spectral analysis, variation of frequency higher than 1 Hz were filtered out using analog filtering circuits. The upper left graphs in Figures 8 and 9 show the power spectra of the surface elevation for Run 1 (begun at 17:10) and Run 2 (begun at 17:20) respectively. The main peak centered at 0.107 Hz is originated from swells. The second peak is originated from wind waves. A straight line affixed to the second peak shows the 'law of $f^{-5}$'. Observed results are well approximated by the law. We notice also that the energy of wind waves in the Run 2 decreased by 14 % compared with that of the Run 1. This energy decrease may be associated with the decrease of the wind speed described above.

The upper right graphs in Figures 8 and 9 show the power spectra of the vertical water velocities. The two spectral peaks, i.e. swells and wind waves, are of nearly equal magnitude in this case. It shows that the swell-peak is located in the '$f^{+1}$' region of amplitude ratio in Figure 3. A straight line noted to the wind wave region shows a slope of the '$f^{-5}$'. Observed results near the wind wave-peak are expressed well by the line and the fact shows that these are located in the 'nearly constant' region in Figure 3 (the amplitude ratio changes slowly from 0.9 to 1.3 in a frequency region of 0.15~0.6 Hz). Slightly steeper region can

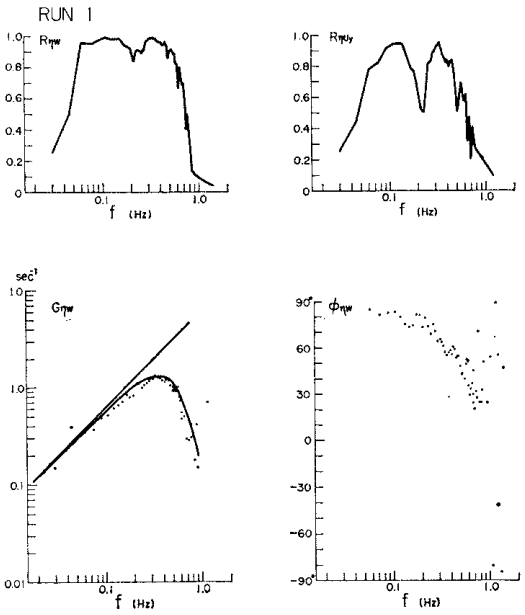


Fig. 10. Frequency response functions estimated for the Run 1: $R_{\eta w}$··· the coherence between the surface elevation and the vertical velocities, $R_{\eta U_y}$··· the coherence between the surface elevation and the horizontal velocities of the $y$-component, $G_{\eta w}$··· the amplitude ratio of the vertical velocities to that of the surface elvation, $\phi_{\eta w}$··· phase difference between the vertical velocities and the surface elevation.

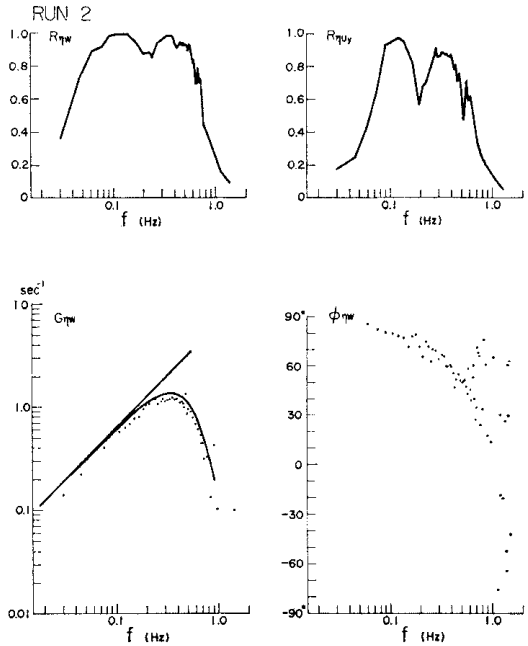


Fig. 11. Frequency response functions estimated for the Run 2: see the caption to Figure 10.

be seen in the highest frequency part.

The lower graphs in the figures show the power spectra of horizontal water velocites. Here the $\bar{x}$-axis is taken in the northeast direction and the $y$-axis is in the northwest direction. The spectral densities of $y$-component are larger than those of $x$-component. The spectral density is proportional to the square of the amplitude of waves in a frequency band. As shown by Eq. (3), the square root of the spectral-density ratio of the $y$-component velocity to the $x$-component velocity approximates the ratio between the two horizontal components of the wavenumber $k_y/k_x$*. By this method, the wave direction was calculated. The wave direction of swell was 71° from the $x$-axis and it agreed with visual estimation by using a "seaman's eye". The direction of wind waves near the spectral peak was 59°. This agrees well with the wind direction of 58° measured with the sonic anemometer for the Run 1.

The upper graphs in Figures 10 and 11 show the coherency of the vertical velocity (left) and the horizontal $y$-component velocity (right) to the surface elevation. The values are nearly equal to 1.0 (the maximums are 0.99) around the spectral peaks. The coherency of $x$-component velocity of the surface elevation, which is not shown in the figures, is lower than that for the $y$-component but exceeds 0.6 near the peaks. These high values of the coherency indicate that the water velocities are mainly associated with the orbital motions of surface waves.

The lower right graphs of Figures 10 and 11 show the phase difference between the surface elevation and the vertical velocity. It is apparent that there is 90°-phase difference as predicted for infinitesimal waves (see Eqs. 3 and 5). At the high frequencies, however, deviation from 90° is observed. This may be caused by the fact that the wave gauge was

* We assumed here that both $k_x$ and $k_y$ are positive. Otherwise, the cross term $\overline{U_x U_y}$ must be taken into consideration (NAGATA, 1964).

set 40 cm apart from the current-meter. The lower left graphs in Figures 10 and 11 show the observed amplitude ratio of the vertical velocities to the surface elevation. The solid curves show the ratio predicted for infinitesimal-amplitude waves of Eq. (5) evaluated for $d=$ 20.0 meters and $z=-1.0$ meter. The observed results agree with the theoretical curve. To examine the relation more closely, the relative magnitude of the observed ratios to the theoretical values was calculated for a frequency region where the value of coherency between the vertical velocities and the surface elevation exceeded 0.8. Figure 12 shows the result where each dot represents the average value of the two runs. The values are nearly constant and the average value of all data in the figure is 0.89, i.e. the observed amplitude of vertical velocity due to orbital motions of surface waves is about 10 % smaller than that described by the infinitesimal-amplitude wave theory.

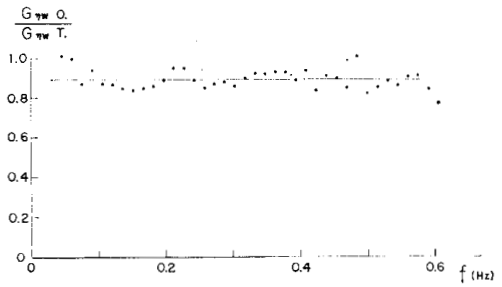


Fig. 12. Relative magnitude of the observed amplitude ratio of the vertical velocities to that of the surface elevation, divided by the theoretical value for infinitesimal-amplitude waves.

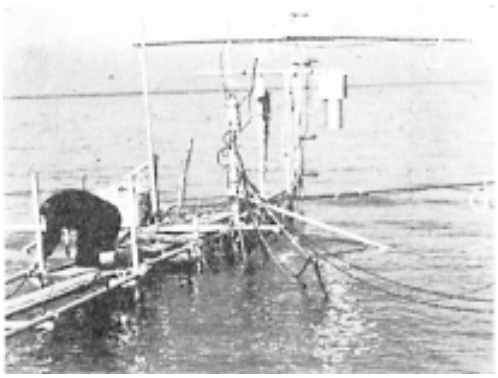

Fig. 13. The observation pier made in the Lake Kasumigaura in 1969.

This difference of 10 % may be significant. The wave gauge and the Doppler current-meter were calibrated immediately before the observations. Instrumental and data-processing errors were expected to be carefully suppressed less than 1 %.

Another series of observations were carried out on a pier (Figure 13) in the Lake Kasumigaura located about 70 km northeast of Tokyo. The Doppler current-meter was arranged in a rugged frame as shown in Figure 14 for the first field observations with it. The meter was immersed at the end of the pier where the water depth was 80.0 cm. The distance from shore was approximately 12 meters. The capacitance wave gauge was attached 50 cm apart from the current-meter.

On 9 December 1969, northwest wind was blowing over the lake from 11:20 a.m. to 11:50 a.m. with the speed of 7.0 m/sec (measured at 1.0 meter height). The fetch was about 9 km for the wind. Five sets of power spectra were computed and one of them is shown in Figure 14. The sampling interval was 0.16 second. Analog filtering circuits were not used. Graphs A and B show spectra of horizontal velocities measured at 30 cm beneath the mean water level. Graph C shows the spectrum of the vertical velocities measured at 45 cm beneath the mean water level. Graph D shows the spectrum of the surface elevation. A solid line in the graph shows the 'law of $f^{-5}$'.

The amplitude ratio between the vertical

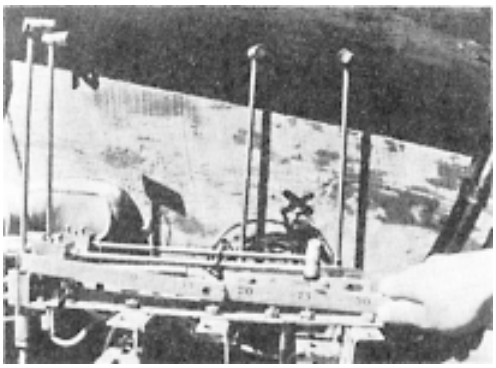

Fig. 14. Sensors of the three-dimensional Doppler current meter arranged in a frame for the lake observation.

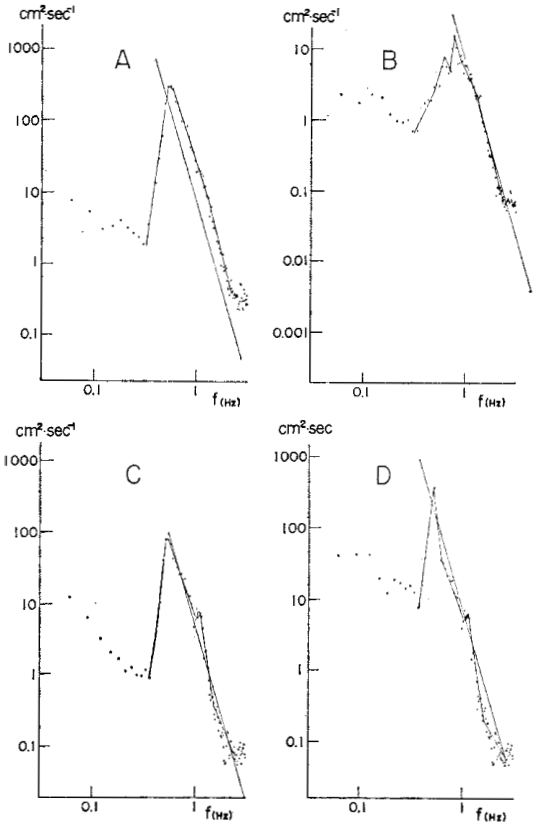


Fig. 15. A set of power spectra for the lake observations: $A$··· the vertical velocities, $B$, $C$··· the horizontal velocities and $D$··· the surface elevation.

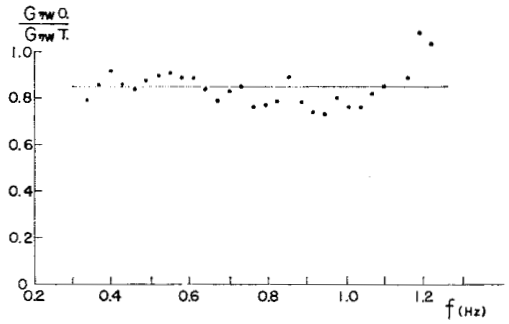


Fig. 16. Relative magnitude of the observed amplitude ratio of the vertical velocities to that of the surface elevation, divided by the theoretical value for infinitesimal-amplitude waves.

velocity and the surface elevation was also examined. Figure 16 shows the relative magnitude of the observed amplitude ratio to the theoretical value. Each dot represents the average value of the five runs. Plot was made for a frequency region where the values of coherency between the vertical velocities and the surface elevation exceeded 0.6. The average value is 0.84, smaller than the value 0.89 obtained in the marine tower observations. The ratios are rather scattered compared with the results at the tower (Figure 12). Following observational conditions are different from those at the marine tower: (a) Wave height of the significant waves $H_{1/3}$ was 25 cm. The ratio of the wave height to the water depth (80.0 cm) is 28 %. Therefore, more intense nonlinearity of water waves is expected. (b) The distance between the wave gauge and the current-meter was 50.0 cm approximately in parallel to wave crests. This was nearly equal to the distance in the tower observations but shorter waves were measured in the lake observations (e.g., wave length was 110 cm for the frequency 1.2 Hz).

The values of coherency between the surface elevation and the vertical velocities are about 0.8 at the low frequencies but the values decrease rather rapidly with frequency. The decrease of the coherency can be regarded as the effects of the short-crestedness of wave trains. The observed amplitude ratios, however, were little affected by the difference in the coherency (0.6 vs. 0.99) as readily shown in Figures 12 and 16. The difference between 0.89 and 0.84 for two cases may be, to some extent, due to the difference in strength of nonlinear interaction of waves of different frequencies.

## 5. Summary and discussions

1. Water velocities in wave fields measured with a Doppler currentmeter are mainly associated with orbital motions of the surface waves. Power spectra of the velocities are well described qualitatively by the theory for infinitesimal-amplitude waves. High values of the coherency between the surface elevation and the water velocities are observed. The phase difference between the surface elevation and

the vertical water velocities is approximately 90°, as would be expected by the theory.

2. For a given surface elevation, the amplitude of the vertical velocities is found to be about 10 % smaller than that would be expected by the theory for infinitesimal-amplitude waves. The average ratios of the observational values to the theoretical values are 0.89 for the marine tower observations and 0.84 for the lake observations. It is suspected that more intense nonlinear effect in wave motion was taking place in the latter case because wave heights were larger and the water depth was shallower than those in the former case.

The amplitude ratio of the pressure variation to the surface elevation has been examined experimentally by many workers and found to be 0.73–0.93 (HOM-MA *et al.* 1965, HISHIDA *et al.* 1969). These values are in good agreement with our result, if one consider that the square of velocity ratio should be compared to the pressure ratio from the dimensional argument. These ratios, therefore, may indicate the degree of nonlinearity of ocean waves.

3. Our newly developed Doppler current-meter, is proved to be able to measure orbital motions for waves shorter than about 110 cm (e.g., 1.2 Hz) with high coherency to the surface elevation. This limit was imposed under rather unfavorable experimental conditions where the decay caused by hydraulic filter was larger and the effect due to the large separation between the wave gauge and the current-meter could not be disregarded. We may expect that velocity fluctuations of scale of a few tens of centimeters can be measured with this current-meter.

## Acknowledgments

The author wishes to express his thanks to Prof. Y. OGURA for his guidance and encouragement throughout the study. Thanks are due to the members of the Hiratsuka Branch of the National Research Center for Disaster Prevention and to all the members of the project for evaporation study represented by Prof. G. YAMAMOTO of Tohoku University.

## References

AKAIKE, H. (1962): On a design principle of lag-window for the estimation of spectra. Annals of the Institute of the Statistical Mathematics. **14**, 1-21.

BARNETT, T. P. and J. C. WILKERSON (1967): On the generation of ocean wind waves as inferred from airborne radar measurements of fetch-limited spectra. J. Marine Res., **25**, 292-328.

BLACKMAN, R. B. and J. W. TUKEY (1958): The measurement of power spectra. Dover Publications, Inc., New York.

COCHRAN, W. T., J. W. COOLEY, D. L. FAVIN, H. D. HELMS, R. A. KAENEL, W. W. LANG, G. C. MALING, D. E. NELSON, C. M. RADER and P. D. WELCH (1967): What is the Fast Fourier Transform ? IEEE Transactions on Audio and Electroacoustics, AU-15, 45-55.

EDGE, B. L. and P. C. LIU (1970): Comparing power spectra computed by Blackman-Tukey and Fast Fourier Transform. Water Resources Res., **6**, 1601-1610.

HISHIDA, K., T. TADA and S. KOIZUMI (1969): On the attenuation of surface waves with depth. Umi to Sora, **44**, 39-45. (In Japanese).

HOM-MA, M., K. HORIKAWA and S. KOMORI (1966): Response characteristics of underwater wave gauge. Proceedings of the 10th Conference on Coastal Engineering.

IWATA, N. and T. TANAKA (1970): Spectral development of wind waves. Kokuritsu Bosai Kagaku-gijutsu Senta Kenkyu Hokoku, **4**, 1-21. (In Japanese).

KOCZY, F. F., M. KRONENGOLD and J. M. LOEWENSTEIN (1962): A Doppler current meter. ISA Mar. Sci. Instr., **2**, 127-134.

KRONENGOLD, M. and W. VLASAK (1965): A Doppler current meter. ISA Mar. Sci. Instr., **3**, 237-250.

MUNK, W. H., F. E. SNODGRASS and M. J. TUCKER (1958): Spectra of low-frequency ocean waves. Bull. Scripps Inst. Oceanog., **7**, 283-362.

NAGATA, Y. (1964): Observations of the directional wave properties. Coastal Engineering in Japan, **7**, 11-30.

PHILLIPS, O. M. (1966): The dynamics of the upper ocean. Cambridge University Press.

SHONTING, D. H. (1964): A preliminary investigation of momentum flux in ocean waves. Pure Appl. Geophys., **57**, 149-152.

SHONTING, D. H. (1967): Measurements of particle motions in ocean waves. J. Marine Res., **25**, 162-181.

SHONTING, D. H. (1968): Autospectra of observed particle motions in wind waves. J. Marine Res., **26**, 43-65.

SHONTING, D. H. (1970): Observations of Reynolds stresses in wind waves. Pure Appl. Geophys., **81**, 202 210.

SNYDER, R. L. and C. S. COX (1966): A field study of the wind generation of ocean waves. J. Marine Res., **24**, 141-178.

TAIRA, K. (1971): Measurements of momentum transfer from air to sea. Proceedings of the Joint Oceanographic Assembly, 1970, Tokyo.

TAIRA, K., A. TAKEDA and K. ISHIKAWA (1971): A Shipborne wave recording system using a digital process. J. Oceanog. Soc. Japan, **27**, 175-186.

WISEMAN, W. J. (1969): On the structure of high-frequency turbulence in a tidal estuary. Chesapeake Bay Institute Tech. Rept. No. 59.

YEFIMOV, V. V. and G. N. KHRISTOFOROV (1969): Izv., Atmos. and Oceanic Phys., **5**, 1036-1048.

ZALKAN, R. L. (1968): Observation of high frequency internal waves in the Pacific Ocean. Ph. D. Theses, Univ. California, San Diego.

## Appendix: Fast Fourier transform method of computing power spectrum

A method for using fast Fourier transform (COCHRAN *et al.* 1967) to reduce the number of arithmetic operations and, therefore the time required for computing a power spectrum is present. By the use of a 'spectral window', each estimate computed by this method has the same frequency resolution and degrees of freedom as those computed by the methods of lagged products technique. Estimates were compared by analyzing a time series of wind-wave data observed at a marine tower. The fast Fourier transform method proved to give the same results as the methods of lagged products technique. The time required for computing the spectrum by the method was a tenth of that by the others.

1. Consider a discretely-sampled, time series of finite length, $X[j\cdot\Delta t]$; $j=0, 1, 2, \ldots, N-1$, where $\Delta t$ is the sampling interval. The basic step in the methods of lagged products technique for the computation of the raw spectral estimate $V_r$ is the Fourier transformation of the autocovariance terms, $C_r$:

$$V_r=\Delta t\left[C_0+2\sum_{q=1}^{M-1}C_q\cdot\cos\frac{qr}{M}\pi+C_M\cos r\pi\right] \qquad (1)$$

The autocovariance terms for the time series are defined by

$$C_r=\frac{1}{N}\sum_{j=0}^{N-1}\{X[(j+r)\cdot\Delta t]-\bar{X}\}\{X[j\cdot\Delta t]-\bar{X}\} \qquad r=0, 1, 2, \ldots, M \qquad (2)$$

where

$$\bar{X}=\frac{1}{N}\sum_{j=0}^{N-1}X[j\cdot\Delta t]$$

$$X[j\cdot\Delta t]=\begin{cases}X[j\cdot\Delta t] & \text{for } j\leqq N-1\\ 0 & \text{for } j>N-1\end{cases}$$

The large fluctuation (including some negative values) associated with the raw estimates, $V_r$, is reduced by means of a 'spectral window', $a_n$. We have the spectral densities at the frequencies as

$$\Phi\left(\frac{r}{M}\cdot\frac{1}{2\Delta t}\right)=\sum_{n=-k}^{k}a_n V_{r+n} \qquad (3)$$

AKAIKE (1962) proposed following 'spectral windows',

$$W1:\ a_0=0.5132,\ a_{\pm1}=0.2434\ (k=1) \qquad (4)$$

$$W3:\ a_0=0.7029,\quad a_{\pm1}=0.2228,\quad a_{\pm2}=-0.0891,\quad a_{\pm3}=0.0149\ (k=3) \qquad (5)$$

MUNK *et al.* (1958) adopted a 'lag window' and the spectral densities are computed by the relation

$$\Phi\left(\frac{k}{M}\cdot\frac{1}{2\Delta t}\right)=\Delta t\cdot\delta_{k,l}\sum_{l=0}^{M}2C_l\left(1+\cos\frac{\pi l}{M}\right)\cos\frac{k\pi l}{M} \qquad (6)$$

where $\delta_{k,l}=1/2$ for $l$, $k=0, M$ and $\delta_{k,l}=1$ otherwise. The spectral densities $\Phi$ follow a chi-square distribution with $\nu$ degrees of freedom. Here $\nu$ is approximated by $2N/M$ (MUNK, *et al.* 1958).

In the fast Fourier transform method, the time series is transformed into a Fourier series

$$X[j\cdot\Delta t]=\sum_{i=0}^{N/2}\left(A_i\cos\frac{2\pi}{N}ij+B_i\sin\frac{2\pi}{N}ij\right) \quad (7)$$

where Fourier coefficients are

$$A_i=\frac{2}{N}\sum_{j=0}^{N-1}X[j\cdot\Delta t]\cos\frac{2\pi}{N}ij,\quad i=1, 2, \ldots, \frac{N}{2}-1$$

$$B_i=\frac{2}{N}\sum_{j=0}^{N-1}[j\cdot\Delta t]\sin\frac{2\pi}{N}ij,\quad i=1, 2, \ldots, \frac{N}{2}-1$$

$$A_0=\frac{1}{N}\sum_{j=0}^{N-1}X[j\cdot\Delta t],$$

$$A_{N/2}=\frac{1}{N}\sum_{j=0}^{N-1}(-1)^jX[j\cdot\Delta t]$$

$$B_0=B_{N/2}=0 \quad (8)$$

The coefficient $A_0$ represents the mean value of the time series, $\bar{X}$. The covariance $C_0$ is obtained by

$$C_0=\frac{1}{N}\sum_{j=0}^{N-1}\{X[j\cdot\Delta t]-A_0\}^2=\frac{1}{2}\sum_{i=0}^{N/2}(A_i^2+B_i^2) \quad (9)$$

We define spectral estimates $P_i$ with two degrees of freedom by

$$P_i=\frac{1}{2}(A_i^2+B_i^2)\cdot\Delta t\cdot\frac{N}{2}\quad i=1, 2, 3, \ldots, \frac{N}{2} \quad (10)$$

To increase spectral stability, a sum over adjacent frequency bands (from $p$ to $q$) is formed, and the number of frequencies included in the sum is $a=q-p+1$. Spectral density with $2a$ degrees of freedom is computed at the central frequency of the band as

$$\Phi\left(\frac{r}{N}\cdot\frac{1}{\Delta t}\right)=\frac{1}{a}\sum_{i=p}^{q}P_i \quad (11)$$

where $r=r_s, 2r_s, 3r_s, \ldots, mr_s$ and $p+q=2r$ The number of frequencies to which estimates are computed is $m$.

In our software, the numerical parameters are $N=2048$, $r_s=10$, $m=102.4$ and $a=19$. We have at the first frequency of $r=r_s=10$,

$$\Phi\left(\frac{10}{1024}\cdot\frac{1}{2\Delta t}\right)=\frac{1}{19}\sum_{i=1}^{19}P_i$$

and at the second frequency of $r=2r_s=20$,

$$\Phi\left(\frac{20}{1024}\cdot\frac{1}{2\Delta t}\right)=\frac{1}{19}\sum_{i=11}^{29}P_i$$

Overlapping average acts as a 'spectral window' which gives the same frequency resolution for given degrees of freedom as the methods of lagged products technique.*

2. For a time series of wind-wave data observed at a marine tower, spectral estimates were computed by the four methods described by Eqs. (4), (5), (6) and (11), respectively. The former two are 'spectral window' methods and the third is 'lag window' method of lagged products technique. The fourth is the fast Fourier transform method. The numerical parameters were $N=2048$, $M=100$ and $m=102.4$. Figure A1 shows the spectral densities computed by the first (4) and the fourth (11). Good agreement is shown for all the frequencies. The spectral densities around the main peak of the figure are tabulated in Table 1. The

* ZALKAN (1968) makes non-overlapping average. Edge and Liu (1970) adopt a method in which the time series are broken into some subseries and the raw spectral estimate is calculated from each subseries. The average of the raw estimates gives the reliable estimates. In both the two cases, the frequency resolution is half of that computed by the methods of lagged products technique.

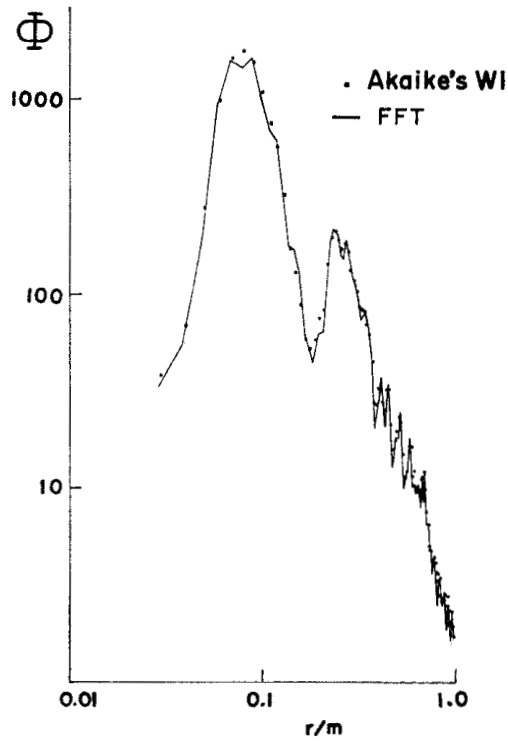


Fig. A1. Power spectra computed by Akaike's W1 (dots) and by the fast Fourier transform method (solid line) for the same data of ocean waves.

Table A1. Power spectral densities of the ocean waves corresponding to the lower frequency peak in Figure 1, computed by the four methods.

| r | (4) | (5) | (6) | (11) |
|---|---|---|---|---|
| 6 | 983 | 999 | 957 | 977 |
| 7 | 1647 | 1816 | 1605 | 1578 |
| 8 | 1769 | 1838 | 1737 | 1458 |
| 9 | 1584 | 1683 | 1537 | 1621 |
| 10 | 1078 | 1011 | 1080 | 1055 |
| 11 | 750 | 697 | 725 | 704 |
| 12 | 576 | 619 | 570 | 626 |
| 13 | 326 | 293 | 326 | 333 |
| 14 | 173 | 139 | 177 | 183 |
| 15 | 131 | 137 | 133 | 172 |
| 16 | 89 | 87 | 95 | 131 |
| 17 | 60 | 53 | 63 | 65 |
| 18 | 53 | 51 | 53 | 56 |
| 19 | 57 | 56 | 55 | 47 |
| 20 | 67 | 67 | 65 | 64 |

values computed by (4) are nearly equal to those by (6). Equivalent 'spectral window' to the 'lag window' of (6) is called 'Hanning' (BLACKMAN and TUKEY, 1958) whose weights are 0.25, 0.50 and 0.25.

The comparison proves that the fast Fourier transform method produces the same results as the lagged products technique. The actual calculations were performed on an OKITAC-5090 digital computer at the Ocean Research Institute, University of Tokyo. The time required for computation was 60 minutes by the methods of (4) or (5), and 95 minutes by the method of (6). On the other hand, the time was only 5 minutes by the fast Fourier transform method of (11).

3. In the fast Fourier transform method, the time series to be analyzed are firstly transformed into Fourier series and we have following convenience: (i) Physical meaning of the spectral estimates is readily examined, especially for a linear problem. (ii) Filtering or integration of the time series can be made by multiplying a weight function of frequencies to the Fourier coefficients. Waveforms after filtering are computed by the inverse Fourier transformation. As application of (ii), TAIRA, TAKEDA and ISHIKAWA (1971) described a method of double integration. They showed the leakage error in a finite Fourier series.

Co-spectrum $C_{XY}$ and quadrature spectrum $Q_{XY}$ between the two time series

$$X[j\cdot\Delta t]=\sum_{i=0}^{N/2}\left\{A_i(X)\cos\frac{2\pi}{N}ij+B_i(X)\sin\frac{2\pi}{N}ij\right\}$$

and

$$Y[j\cdot\Delta t]=\sum_{i=0}^{N/2}\left\{A_i(Y)\cos\frac{2\pi}{N}ij+B_i(Y)\sin\frac{2\pi}{N}ij\right\}$$

$$j=0, 1, 2, \ldots, N-1$$

are computed in the same manner as the power spectrum:

$$C_{XY}\left(\frac{r}{N}\cdot\frac{1}{\Delta t}\right)=\frac{N\cdot\Delta t}{4a}\sum_{i=p}^{q}\{A_i(X)A_i(Y)+B_i(X)B_i(Y)\} \quad (12)$$

$$Q_{XY}\left(\frac{r}{N}\cdot\frac{1}{\Delta t}\right)=\frac{N\cdot\Delta t}{4a}\sum_{i=p}^{q}\{A_i(X)B_i(Y)-A_i(Y)B_i(X)\} \quad (13)$$

The estimates of the coherence and the phase difference are:

$$R^2_{XY}\left(\frac{r}{N}\cdot\frac{1}{\Delta t}\right)=\frac{C^2_{XY}\left(\frac{r}{N}\cdot\frac{1}{\Delta t}\right)+Q^2_{XY}\left(\frac{r}{N}\frac{1}{\Delta t}\right)}{\Phi_X\left(\frac{r}{N}\cdot\frac{1}{\Delta t}\right)\cdot\Phi_Y\left(\frac{r}{N}\frac{1}{\Delta t}\right)} \quad (14)$$

and

$$\phi_{XY}\left(\frac{r}{N}\frac{1}{\Delta t}\right)=\tan^{-1}\left\{Q_{XY}\left(\frac{r}{N}\frac{1}{\Delta t}\right)\Big/C_{XY}\left(\frac{r}{N}\frac{1}{\Delta t}\right)\right\} \quad (Y \text{ leads } X.) \quad (15)$$

The 'gain', i.e. the amplitude ratio of $Y$ to $X$ is

$$G_{XY}\left(\frac{r}{N}\frac{1}{\Delta t}\right)=\left\{C^2_{XY}\left(\frac{r}{N}\frac{1}{\Delta t}\right)+Q^2_{XY}\left(\frac{r}{N}\frac{1}{\Delta t}\right)\right\}^{\frac{1}{2}}\Big/\Phi_X\left(\frac{r}{N}\frac{1}{\Delta t}\right) \quad (16)$$

Consider a special case in which each time series is a single sinusoidal wave train; $X[j\cdot\Delta t]=\alpha\cos\frac{2\pi}{N}ij$, $Y[j\cdot\Delta t]=\beta\sin\left(\frac{2\pi}{N}ij+\theta\right)$. The Fourier coefficients are

$$A_i(X)=\alpha, \qquad B_i(X)=0$$
$$A_i(Y)=\beta\sin\theta, \quad B_i(Y)=\beta\cos\theta$$

Power spectra and cross-spectra are described as

$$\Phi_X=\alpha^2$$
$$\Phi_Y=\beta^2$$
$$C_{XY}=\alpha\beta\sin\theta$$
$$Q_{XY}=\alpha\beta\cos\theta$$

For simplicity, we omitted a constant multiplier. Note that power spectra represent the squares of amplitudes and that co-spectra and quadrature-spectra represent the products of in-phase components and 90°-phase components respectively. By using the spectra, phase lag and gain are obtained as

$$\phi_{XY}=\tan^{-1}(\cos\theta/\sin\theta)=\frac{\pi}{2}-\theta$$
$$G_{XY}=\beta/\alpha$$

The phase lag can be readily shown by the graphical relation in this case. The gain represents the amplitude ratio between the two waveforms.

Coherence $R^2_{XY}$ calculated from spectra with two degrees of freedom is always unity. To avoid this triviality, coherence is defined for averaged spectra over a frequency band. We assume that the Fourier coefficients are sum of constants and noise term:

$$A_i(X)=\frac{\alpha}{\sqrt{2a}}+\gamma_i, \quad B_i(X)=0$$
$$A_i(Y)=\frac{\beta}{\sqrt{2a}}+\delta_i, \quad B_i(Y)=0$$
$$\sum_{i=p}^{q}\gamma_i=\sum_{i=p}^{q}\delta_i=\sum_{i=p}^{q}\delta_i\gamma_i=0$$

where $p\leqq i\leqq q$ and $a=q-p+1$. Omitting again the constant multiplier, we have spectral estimates as

$$\Phi_X=\alpha^2+\sum_{i=p}^{q}\gamma_i^2, \quad C_{XY}=\alpha\beta$$
$$\Phi_Y=\beta^2+\sum_{i=p}^{q}\delta_i^2, \quad Q_{XY}=0$$

By the formula, we have: $R^2_{xy}=1.0$ for $\sum_{i=p}^{q}\gamma_i^2=\sum_{i=p}^{q}\delta_i^2=0$, $R^2_{xy}\to 0$ for $\sum_{i=p}^{q}\gamma_i^2/\alpha^2\to\infty$ and/or $\sum_{i=p}^{q}\delta_i/\beta^2\to\infty$. The value of coherence varies between 0 and 1, and it shows degree of contamination by noise. Consider a more special case:

$$\sum_{i=p}^{q} \gamma_i^2/\alpha^2 = \sum_{i=p}^{q} \delta_i^2/\beta^2 = \varepsilon$$

we have

$$R^2_{XY} = \frac{1}{(1+\varepsilon)^2}$$

Figure A2 illustrates the coherence as a function of the power ratio of the noise to that of the signal. The value of coherence decreases as the ratio increases. It is noteworthy that the case of $R=0.5$, which we sometimes take as a criterion for the significance of correlation between the two signals, corresponds to $\varepsilon=1.0$ in this special case. Let us consider the case where $\alpha=\beta$, then the gain $G_{XY}$ is unity when the noise vanishes as we have shown. For this case, however, we have

$$G_{XY} = \frac{1}{1+\varepsilon} = R.$$

The estimates of the gain are also affected by the noise.

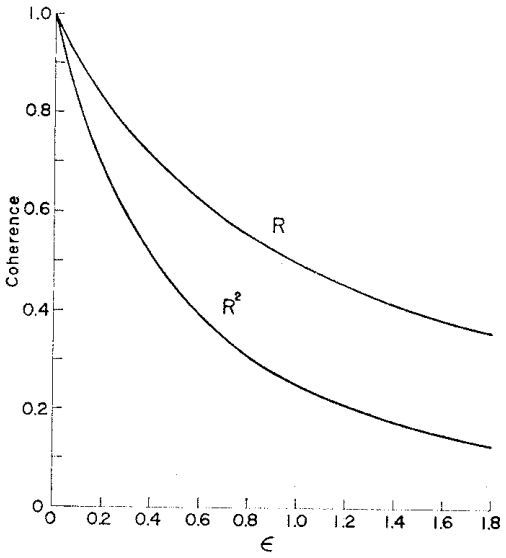


Fig. A2. The estimates of the coherence for a case where the signals are contaminated by the noise, ε represents the power ratio of the noise to the signals.

# ドップラー流速計で測定した波浪場の流速変動

平　　啓　介

**要旨**　新しく開発した超音波ドップラー式三次元流速計を用いて，波浪場の流速変動を測定した．防災センター平塚波浪観測塔（流速計は海面下 1.0 m に設置）および霞ケ浦南岸（水面下 0.45 m に計置）において野外観測を行なった．流速値と同時に表面波形も記録し，両者の振巾および位相関係をスペクトル解析を行なって調べた．観測結果を微小振巾波理論と比較し，流速変動が主として表面波の軌道運動によって生じていることがわかった．流速の鉛直成分と表面波形との位相差は 90° で理論値とよくあうが，流速変動の振巾は表面波影の振巾より約 10 % 小さいことが示された．

この研究で採用したスペクトル解析法は FFT 法であるが，Blackman-Tukey 法と自由度および分解能を同じにする工夫がなされている．この方法，ならびに風浪のデータについて 4 通りの方法によってパワースペクトルを算出した相互比較についても記述した．